Individual nanocomposite sheets of chemically reduced graphene oxide and poly(*N*-vinyl pyrrolidone): preparation and humidity sensing characteristics†

Jiali Zhang, Guangxia Shen, Wanjun Wang, Xuejiao Zhou and Shouwu Guo*

Received 28th July 2010, Accepted 8th September 2010
DOI: 10.1039/c0jm02440f

Individual nanocomposite sheets of chemically reduced graphene oxide (CRG) and poly(*N*-vinyl pyrrolidone) (PVP), namely CRG/PVP, have been fabricated through a simple one-pot procedure. The structure and composition of the as-prepared CRG/PVP sheets were complementarily characterized using solid-state ^{13}C NMR, atomic force microscopy (AFM), X-ray photoelectron spectroscopy (XPS), differential scanning calorimetry (DSC), thermogravimetric analysis (TGA), and other spectroscopic measurements, demonstrating that the PVP molecules were chemically grafted on the CRG surfaces. The electrical conductivity of the individual CRG/PVP sheets was measured at different levels of relative humidity (RH) using a conductive atomic force microscopy (CAFM) system, revealing that the electrical conductivity of a CRG/PVP sheet is sensitive to RH variation with a response time of a few seconds. Given the easy mass scale production and improved electrical conductivity, we envisage that the CRG/PVP nanocomposite sheets should have a broad spectrum of applications in electrical conductivity based sensors.

Introduction

Graphene sheets, due to their unique two-dimensional structure, exceptional electrical and mechanical properties, and potential applications, have attracted substantial attention during the last few years.[1–3] Individual graphene sheets have been prepared successfully at the laboratory scale through micromechanical exfoliation of graphite,[2] chemical vapor deposition (CVD),[4,5] and expitaxial growth.[6,7] However, the preparation of high quality graphene sheets in mass scale production is still challenging. In addition, the lack of surface functionalities, which can serve as anchoring sites for external molecules and other species on pristine graphene sheets, sometimes limits the application of graphene, for example, in the use of graphene sheets as sorption-based sensors.[8–11] In comparison, graphene oxide (GO) sheets have abundant oxygen-containing surface groups, including epoxide, hydroxyl, and carboxylic groups, and can be fabricated from graphite in bulk-scale production.[12–17] Nonetheless, as the conjugated electronic state is interrupted, the GO sheet exhibits poor electrical conductivity, which is a real drawback for its applications in electrical conductance based devices. Therefore, more recently, a lot of effort has been made to develop methods for either thoroughly reducing GO to graphene to restore the conjugated electronic state of GO, or chemically modifying graphene surfaces to make them more suitable for use in devices. For instance, it has been reported that the hydrazine,[16] hydroquinone,[18] $NaBH_4$,[19,20] and other physical reduction methods[21–23] can efficiently reduce GO, forming electrically conducting CRG. It has also been demonstrated that the chemically derived surfaces of graphene and CRG sheets could tailor their electrical,[24] optical,[25] mechanical[26] properties, and biological/chemical compatibilities,[27,28] though the binding state of the attached molecules on the graphene and CRG surfaces, and the detailed interaction mechanism between graphene or CRG and the attached molecules are remains to be elucidated.

In our recent work, we have demonstrated that the atomically flat surface of GO makes it possible to monitor *in situ* the adsorption of the enzyme molecules on the GO surface using atomic force microscopy (AFM) providing an insight into the interactions between enzyme molecules and GO.[29,30] We have also shown that the oxygen containing groups on GO surface could be reduced using L-ascorbic acid (L-AA), resulting in the restoration of the conjugated electronic state and the electrical conductivity of the CRG sheets.[31] It has long been illustrated that the pyrrolidone units afford poly(*N*-vinyl pyrrolidone) (PVP) with unique biocompatibility, high water-solubility, and, more attractively, a strong affinity for widespread biological and chemical species.[32] Therefore, PVP has often been utilized to modify the surfaces of carbon nanotubes and other nanoparticles to enhance their surface functionalities.[33,34] Herein, we report a facile approach to fabricate individual nanocomposite sheets of CRG with PVP (CRG/PVP). As will be shown, using the atomically flat surface of CRG, we can not only observe the PVP grafted on the CRG, but can also monitor the adsorption of water and other molecules on CRG/PVP. More significantly, we found the CRG/PVP sheets exhibit an extraordinary water adsorption capability, and the electrical conductivity of

National Key Laboratory of Micro/Nano Fabrication Technology, Key Laboratory for Thin Film and Microfabrication of the Ministry of Education, Research Institute of Micro/Nano Science and Technology, Shanghai Jiao Tong University, Shanghai, 200240, China. E-mail: swguo@sjtu.edu.cn

† Electronic supplementary information (ESI) available: Preparation of GO; UV-vis absorption spectra of aqueous dispersions containing CRG, PVP, and L-AA acquired at different reaction times; X-ray photoelectron spectroscopy (XPS) spectra in C 1s of GO, bare CRG and CRG/PVP Raman spectra of GO and CRG/PVP; and a tapping mode AFM image of CRG/PVP sheets after being kept in a basic aqueous solution with pH 10 for 12 h. See DOI: 10.1039/c0jm02440f

a CRG/PVP sheet is exceptionally sensitive to the relative humidity. The as-prepared CRG/PVP is potentially an ideal nanoscale material for sorption and electrical conductance based humidity sensor.

Experimental section

Preparation of CRG/PVP

Graphene oxide was prepared using nature graphite powders as the raw material through a modified Hummers method.[35,36] The details were presented in the electronic supplementary information (ESI, †). For preparation of individual CRG/PVP sheets, in a typical experiment, 0.05 g of PVP (MW, 40 kg mol^{-1}) and 0.1 g of L-ascorbic acid were added to 200 mL, 0.25 mg mL^{-1} of GO aqueous solution at the same time. The mixture was stirred first for 10 min at room temperature (~23 °C), and then 4 h at 80 °C. A stable homogeneous black suspension was obtained. The black solid product was separated from the reaction mixture through filtration, washed three times with deionized water, and finally redispersed in deionized water for further usage.

Characterization

UV-vis spectra were carried out using a UV-2550 UV-vis spectrometer (Shimadzu, Japan). The aqueous dispersions of GO or CRG/PVP were used for the UV-vis measurements, and the pure water served as reference. Solid state ^{13}C magic-angle spinning (MAS) NMR spectra were obtained on an Avance III 400 NMR (Bruker, Germany) with ^{1}H-^{13}C cross polarization. TGA curves were recorded on a TGA 7 thermogravimetric analyzer (Perkin Elmer, USA) at a heating rate of 10 °C min^{-1} under nitrogen flow. DSC curves were acquired on a differential scanning calorimeter (Diamond, Perkin Elmer, USA) at a heating rate of 10 °C min^{-1} under nitrogen flow. Atomic force microscopic (AFM) images of graphene oxide and CRG/PVP were taken on a MultiMode Nanoscope V scanning probe microscopy system (Veeco, USA). Commercially available AFM cantilever tips with a force constant of ~ 48 N m^{-1} and resonance vibration frequency of ~ 330 kHz were used. The scanning rate was set usually at 0.7 to 1 Hz. Raman spectra were obtained on an Invia/Reflrx lasser micro-raman spectroscope (Renishaw, England) with a 514 nm laser beam. XPS measurements were performed on an Axis Ultra DLD X-ray photoelectron spectroscopy (Kratos Analytical, UK) using monochromatic Al Kα (1486.6 eV) source at 15 kV.

Electrical conductivity measurements on CRG/PVP

The electrical conductivity of an individual CRG/PVP sheet was measured with a conductive AFM (C-AFM) system that was performed on a MultiMode Nanoscope V scanning probe microscope equipped with an S/N771 Application Module (Vecco, USA), a SCM-PIC conductive AFM tip was used. The samples for electrical conductivity measurement were prepared simply by spinning-coating the as-prepared CRG/PVP sheets on a freshly cleaved mica substrate. The relative humidity control was realized using a commercially available AFM liquid cell with a small cavity (Vecco, USA).

Results and discussion

The preparation of CRG/PVP individual nanocomposite sheets, including the reduction of GO and the grafting of PVP on CRG, was accomplished through a one-pot procedure. The conversion of GO to CRG in the presence of PVP with L-AA was confirmed by UV-vis, XPS, and Raman spectroscopy (Figures S1, S2, and S3 in ESI†), and the results are similar to those we obtained previously.[31] The formation of CRG/PVP sheets was conclusively determined by solid-state ^{13}C magic-angle spinning (MAS) NMR spectroscopy. In Fig. 1, lines a and b show typical ^{1}H–^{13}C cross polarization (CP) spectra of PVP and CRG/PVP acquired with 5 kHz MAS and a contact time of 2 ms (1024 scans). Four peaks at 176, 43, 32, and 19 ppm from PVP molecules in the ^{13}C NMR spectra of both PVP and CRG/PVP were observed. Unfortunately, we have not observed any typical ^{13}C NMR signal for the graphite carbons of CRG/PVP due to sample spinning and probe tuning problems. As a control experiment, we also ran the ^{13}C NMR measurement for CRG alone. However, as shown in Fig. 1, line c, a ^{13}C NMR signal for graphitic sp^2 carbons was not observed. A similar problem was encountered by other researchers.[13] Nevertheless, the NMR data confirms the formation of CRG/PVP. The morphology of as-prepared CRG/PVP was imaged using AFM. Fig. 2a and c show the tapping mode AFM images of CRG and CRG/PVP sheets. Compared to the smooth and flat surface of the CRG sheets, densely packed nanospheres of almost uniformed size, presumably the PVP, were clearly observed all over the surface of the CRG/PVP sheets. The height profiles of the AFM images of the CRG and CRG/PVP, Fig. 2b and d, show that the average thickness of the CRG/PVP and CRG sheets are ~2.5 and ~0.8 nm, respectively. The thickness difference, ~1.7 nm, should correlate with the average size of the PVP nanospheres on the CRG/PVP.

We demonstrated previously that the GO sheets are negatively charged in an aqueous solution with pH range from 4 to 11.[17] It has also been reported that under acidic condition PVP molecules are positively charged due to the protonation of pyrrolidone groups.[37] Thus, when the L-AA was employed as a reductant, it is likely that an electrostatic attraction contributes to the grafting of PVP onto the GO sheets. However, during the

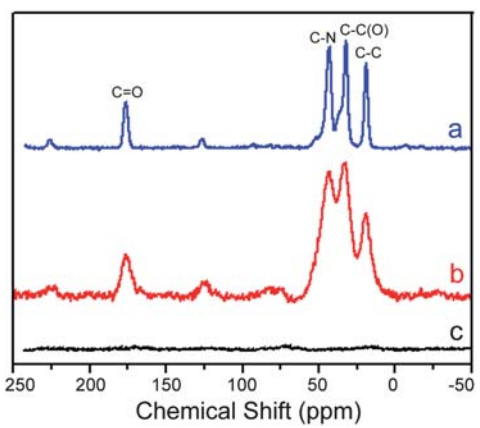

Fig. 1 Solid state ^{13}C magic-angle spinning (MAS) NMR spectra of (a) PVP, (b) CRG-PVP, and (c) CRG.

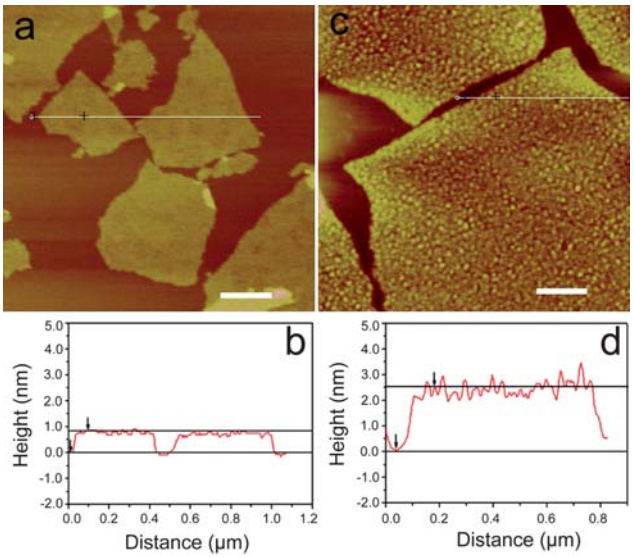

Fig. 2 Tapping mode atomic force microscopy (T-AFM) images of individual (a) CRG and (c) CRG/PVP sheets acquired at a relative humidity (RH) of 30%, and the height profiles of (b) CRG and (d) CRG/PVP sheets. The corresponding thicknesses of CRG and CRG/PVP sheets are ~ 0.8 and 2.5 nm, respectively. The scale bars equal 250 nm.

GO reduction process, the oxygen-containing functional groups on the GO surface were gradually removed, and the negative charge capacity of the GO decreased. When the GO was completely converted to CRG, most of the oxygen-containing groups were removed; and the electrostatic interaction between PVP and GO should be dramatically suppressed. To further explore the contribution of the electrostatic attraction in the interaction between PVP and CRG, we dispersed as-prepared CRG/PVP sheets into an aqueous solution with pH of 10 (both the GO sheet and the PVP molecules should be negatively charged under this condition), and stirred at room temperature for 12 h. The AFM image of the sample showed that the PVP was still bound on the CRG surface (Figure S4†). This implies that the electrostatic interactions might not be the major contributor to the interaction between CRG and PVP. Therefore, as shown in Fig. 3, we propose that certain chemical bonds may be formed between the PVP molecules and some of the oxygen-containing functional groups on GO before it was completely reduced to CRG. Most probably, at the beginning of the reduction, some of the *tert*-amide groups in the pyrrolidones of PVP are protonated by the L-AA activating amide group of PVP. Subsequently, the activated *tert*-amide groups of PVP are attacked by the epoxide or hydroxyl groups of the GO resulting in the amide bond being broken, and the formation of an ester bond. The assumption of covalent bond formation was confirmed by DSC and TGA measurements. Fig. 4a depicts the DSC curves of CRG, CRG/PVP, and PVP. Except for an exothermic peak at ~87 °C corresponding to the glass phase transition of PVP, no other exothermic peaks appeared in the temperatures range from 0 to

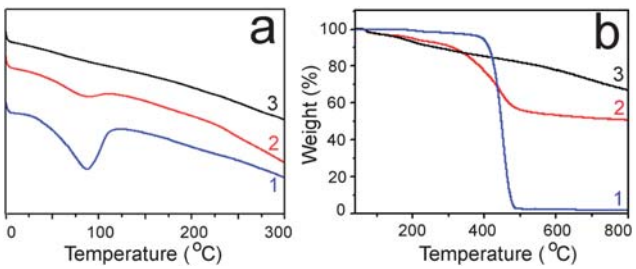

Fig. 4 a) DSC and b) TGA plots of (1) PVP, (2) CRG-PVP, and (3) CRG.

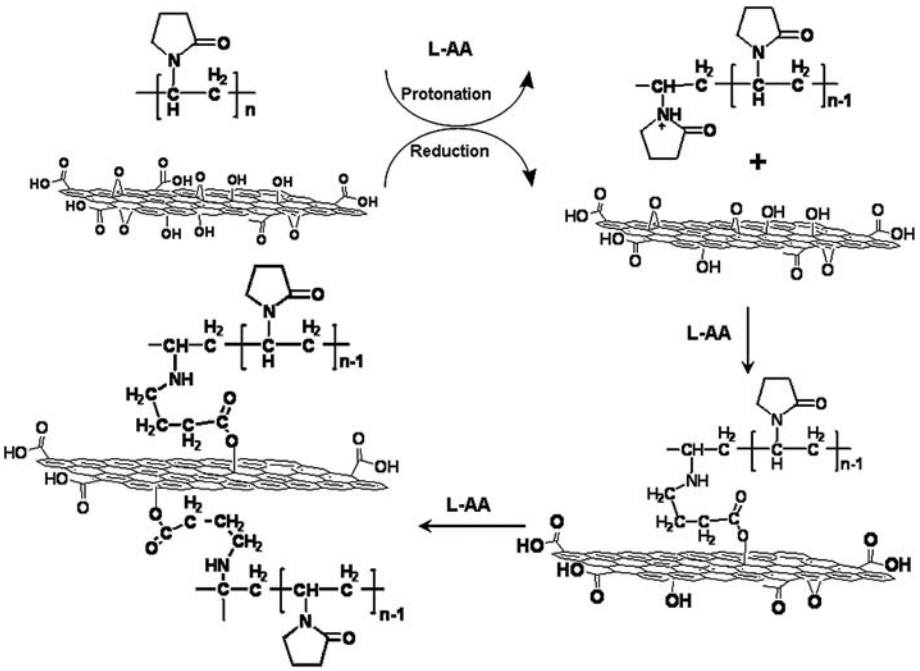

Fig. 3 Schematic representation of a mechanism proposed for the formation of individual CRG/PVP sheet.

300 °C in the CRG/PVP sample, implying that, rather than a weak electrostatic interaction, the PVP molecules bind to the CRG through chemical bonds. This was proved independently by TGA as well. As shown in Fig. 4b, the major mass loss occurs at ~380 °C for CRG/PVP which is slightly lower than that for pure PVP (~410 °C). The overall mass loss of the CRG/PVP is of ~45%, which can be attributed partially (~15%) to the unreduced oxygen-containing groups on CRG (for comparison, see line 3 of Fig. 4b, a TGA curve of the CRG alone),[16,38] and mainly (~30%) to the decomposition of the PVP.

As we mentioned above, the PVP modified carbon nanotubes and other nanoparticles showed novel properties.[33,34] Hence, the properties of individual CRG/PVP nanocomposite sheets should be different from those of the bare CRG sheets. Considering that the PVP has a strong water adsorption capability, the topographic images of as-prepared CRG/PVP sheets were first acquired with AFM under different RH. Fig. 2c, and Fig. 5a and c depict the AFM images of CRG/PVP sheets obtained at different RH of 30%, 60%, and 90%, respectively. We found that the thickness of the CRG/PVP sheets, the height profile of the corresponding AFM image, was increased from 2.5 nm to 3.6 nm with the RH increasing from 30% (Fig. 2d) to 90% (Fig. 5d), revealing that the PVP nanospheres on the CRG were heavily swollen with water. These observations prompted us to investigate further the electrical conductivity of CRG/PVP, and, more attractively, the sensitivity of their electrical conducting performance to RH. To do this, individual CRG/PVP sheets were spinn-coated on a freshly cleaved mica surface, and were heated at 80 °C for 12 h under vacuum (0.01 Torr) to remove water molecules adsorbed on the CRG/PVP. Subsequently, half of the mica substrate surface with CRG–PVP was covered with a thin film of silver (~50 nm of thickness) through simple staining of the conductive silver sol. As shown in the inset of Fig. 6a, using the silver thin film as one

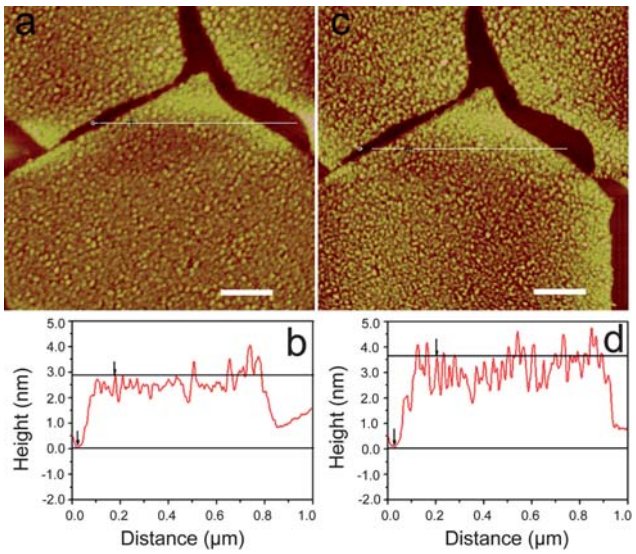

Fig. 5 Tapping mode AFM images of individual CRG/PVP sheets obtained at RH of (a) 60%, and (c) 90%, and height profiles of CRG/PVP sheets at RH of (b) 60%, and (d) 90%. The thicknesses of the CRG/PVP sheet at different RH of 60% and 90% are about 2.9, and 3.6 nm, respectively. The scale bars equal 250 nm.

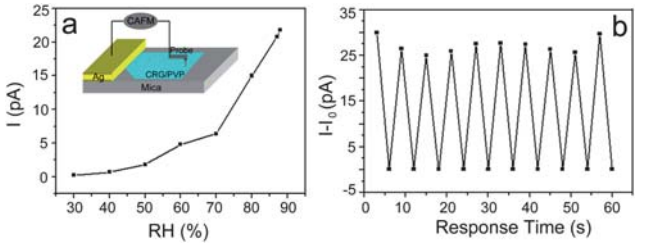

Fig. 6 a) Plots of current (*I*) *versus* RH acquired on an individual CRG/PVP sheet under different RH conditions with a bias of 1 V using C-AFM. b) Real time conductance response to the RH oscillation between 30% and 90% with a bias of 1 V. The RH oscillation was achieved by exposure the CRG/PVP sheet to RH environment with 90% and 30%, alternatively in a chamber equipped with the C-AFM. Inset in (a) shows schematically a two-electrode system based on conductive atomic force microscopy (C-AFM) used for the electrical conductivity measurements of the individual CRG/PVP sheets.

electrode and a conductive atomic force microscopy (C-AFM) tip as the other electrode, a two-electrode electrical conductivity measurement system was built up that was used for the measurement of current (*I*) and voltage (*V*) of individual CRG/PVP sheets. To control the RH, a commercially available AFM liquid cell with a tiny cavity (Veeco, USA) was used. Thus, the RH could be adjusted simply by purging the small cavity of the AFM liquid cell alternatively with pure nitrogen gas or the air of different relative humidity of 30% to 90%. The currents of the CRG/PVP sheets under different RH were obtained by applying a constant bias (voltage) through the C-AFM tip that was connected to a current amplifier. Fig. 6a shows a typical curve of current *versus* RH (*I*–RH curve) acquired on an individual CRG/PVP sheet with a bias of 1 V. Clearly, the electrical conductivity of the CRG/PVP sheets increase with increasing RH. There are two phases in the *I*–RH curve with a constant bias. When the RH is below 70%, the current increases relatively slow with increasing RH; but when the RH is above 70%, the current increases abruptly with increasing RH. Moreover, the utilization of an AFM liquid cell enabled us to vary the RH over the surface of individual CRG/PVP sheets inside the cavity of the AFM liquid cell quickly. Consequently, the response of electrical conductivity of CRG/PVP to the RH variation could be measured. Fig. 6b shows the response of the electrical conductivity of CRG/PVP to the RH changing from 30% to 90% reversibly. The measured response time is within 3 s which is the time limit of the RH change achieved in the AFM liquid cell cavity. In comparison, we measured the electrical conductivity of bare individual CRG sheets under the same conditions, but found that the humidity variation did not affect the electrical conductivity as dramatically as on the CRG/PVP, which is similar to the results reported by others.[9,10] The results lead us to believe that the large amount of water molecules adsorbed by PVP could assist the charge transfer on the CRG/PVP composite sheets. The quick response of the electrical conductivity of the CRG/PVP to the RH change may originate from the rapid adsorption and desorption capability of nanosized PVP particles on CRG to water molecules. This property endows the CRG/PVP with an advantage over graphene and CRG sheets used in molecular sensors, in which external molecules were believed to be adsorbed directly on the defects of the graphene or the residual oxygen containing groups of CRG.[8,11]

Nevertheless, the humidity dependent electrical conductivity of CRG/PVP renders it as an ideal candidate material for humidity sensor.

Conclusion

In summary, individual CRG sheets have been successfully modified by grafting PVP through a simple one-pot approach forming CRG/PVP nanocomposite sheets with improved conductivity. More importantly, the electrical conductivity of the individual CRG/PVP composite sheets is highly sensitive to the relative humidity of the environment, with a response time of ~3 s. The method elaborated in this work will provide an impetus in functionalizing CRG, which should find a broad spectrum of applications including absorption materials, electrical conductance based sensors, or other electronic/electric devices.

Acknowledgements

This work was financially supported by the National "973" Program (Nos. 2007CB936000 and 2010CB933900) and the NSFC (Nos. 20774029, 90923041) of China.

References and notes

1 A. K. Geim and K. S. Novoselov, *Nat. Mater.*, 2007, **6**, 183–191.
2 K. S. Novoselov, A. K. Geim, S. V. Morozov and D. Jiang, *Science*, 2004, **306**, 666–669.
3 C. N. R. Rao, A. K. Sood, K. S. Subrahmanyam and A. Govindaraj, *Angew. Chem., Int. Ed.*, 2009, **48**, 7752–7777.
4 A. Dato, V. Radmilovic, Z. Lee, J. Phillips and M. Frenklach, *Nano Lett.*, 2008, **8**, 2012–2016.
5 K. Kim, Y. Zhao, H. Jang, S. Lee, J. Kim, K. Kim, J. Ahn, P. Kim, J. Choi and B. Hong, *Nature*, 2009, **457**, 706–710.
6 P. Sutter, J. Flege and E. Sutter, *Nat. Mater.*, 2008, **7**, 406–411.
7 J. Hass, W. A. d. Heer and E. H. Conrad, *J. Phys.: Condens. Matter*, 2008, **20**, 323202.
8 J. D. Fowler, M. J. Allen, V. C. Tung, Y. Yang, R. B. Kaner and B. H. Weiller, *ACS Nano*, 2009, **3**, 301–306.
9 A. Ghosh, D. late, L. Panchakarla, A. Govindaraj and C. Rao, *J. Exp. Nanosci.*, 2009, **4**, 313–322.
10 I. Jung, D. Dikin, S. Park, W. Cai, S. L. Mielke and R. S. Ruoff, *J. Phys. Chem. C*, 2008, **112**, 20264–20268.
11 J. T. Robinson, F. K. Perkins, E. S. Snow, Z. Wei and P. E. Sheehan, *Nano Lett.*, 2008, **8**, 3137–3140.
12 D. Dreyer, S. Park, C. Bielawski and R. Ruoff, *Chem. Soc. Rev.*, 2010, **39**, 228–240.
13 W. Gao, L. B. Alemany, L. Ci and P. M. Ajayan, *Nat. Chem.*, 2009, **1**, 403–408.
14 D. Li, M. B. Muller, S. Gilje, R. B. Kaner and G. G. Wallace, *Nat. Nanotechnol.*, 2008, **3**, 101–105.
15 S. Park and R. s. Ruoff, *Nat. Nanotechnol.*, 2009, **4**, 217–224.
16 S. Stankovich, D. A. Dikin, R. D. Piner, K. A. Kohlhaas, A. Kleinhammes, Y. Jia, Y. Wu, S. T. Nguyen and R. S. Ruoff, *Carbon*, 2007, **45**, 1558–1565.
17 V. C. Tung, M. J. Allen, Y. Yang and R. B. Kaner, *Nat. Nanotechnol.*, 2008, **4**, 25–29.
18 R. Hao, W. Qian, L. Zhang and Y. Hou, *Chem. Commun.*, 2008, 6576–6578.
19 R. Muszynski, B. Seger and P. V. Kamat, *J. Phys. Chem. C*, 2008, **112**, 5263–5266.
20 Y. Si and E. T. Samulski, *Nano Lett.*, 2008, **8**, 1679–1682.
21 H. Li, S. Pang, X. Feng, K. Müllen and C. Bubeck, *Chem. Commun.*, 2010, **46**, 6243–6245.
22 Y. Liang, J. Frisch, L. Zhi, H. Norouzi-Arasi, X. Feng, J. P. Rabe, N. Koch and K. Müllen, *Nanotechnology*, 2009, **20**, 434007.
23 Q. Su, S. Pang, V. Alijani, C. Li, X. Feng and K. Müllen, *Adv. Mater.*, 2009, **21**, 3191–3195.
24 F. Chen and N. J. Tao, *Acc. Chem. Res.*, 2008, **42**, 429–438.
25 Y. Xu, Z. Liu, X. Zhang, Y. Wang, J. Tian, Y. Huang, Y. Ma, X. Zhang and Y. Chen, *Adv. Mater.*, 2009, **21**, 1275–1279.
26 C. Gomez-Navarro, R. T. Weitz, A. M. Bittner, M. Scolari, A. Mews, M. Burghard and K. Kern, *Nano Lett.*, 2007, **7**, 3499–3503.
27 Z. Liu, J. T. Robinson, X. Sun and H. Dai, *J. Am. Chem. Soc.*, 2008, **130**, 10876–10877.
28 J. R. Lomeda, C. D. Doyle, D. V. Kosynkin, W.-F. Hwang and J. M. Tour, *J. Am. Chem. Soc.*, 2008, **130**, 16201–16206.
29 F. Zhang, B. Zheng, J. Zhang, X. Huang, H. Liu, S. Guo and J. Zhang, *J. Phys. Chem. C*, 2010, **114**, 8469–8473.
30 J. Zhang, F. Zhang, H. Yang, X. Huang, H. Liu, J. Zhang and S. Guo, *Langmuir*, 2010, **26**, 6083–6085.
31 J. Zhang, H. Yang, G. Shen, P. Cheng, J. Zhang and S. Guo, *Chem. Commun.*, 2010, **46**, 1112–1114.
32 A. B. Bourlinos, V. Georgakilas, R. Zboril, T. A. Steriotis, A. K. Stubos and C. Trapalis, *Solid State Commun.*, 2009, **149**, 2172–2176.
33 L.-J. Li, R. J. Nicholas, C.-Y. Chen, R. C. Darton and S. C. Baker, *Nanotechnology*, 2005, **16**, S202–S205.
34 X. Yang, N. Yan, Z. Fei, R. M. Crespo-Quesada, G. Laurenczy, L. Kiwi-Minsker, Y. Kou, Y. Li and P. J. Dyson, *Inorg. Chem.*, 2008, **47**, 7444–7446.
35 W. S. Hummers, JR. and R. E. Offeman, *J. Am. Chem. Soc.*, 1958, **80**, 1339.
36 G. I. Titelman, V. Gelman, S. Bron, R. L. Khalfin, Y. Cohen and H. Bianco-Peled, *Carbon*, 2005, **43**, 641–649.
37 G. Ster and E. H. Immergut, *J. Am. Chem. Soc.*, 1954, **76**, 1393–1396.
38 L. J. Cote, R. Cruz-Silva and J. Huang, *J. Am. Chem. Soc.*, 2009, **131**, 11027–11032.

